PAPER

Check for updates

Vertical Bi$_2$Se$_3$ flake array as a Pt-free counter electrode for dye-sensitized solar cells†

Manshu Han, Shuang Lu, Jiangang Ma, [ID]* Haiyang Xu, [ID]* Yinglin Wang, Xintong Zhang [ID] and Yichun Liu

In dye-sensitized solar cells (DSSCs), the catalytic activity and electrical conductivity of the counter electrodes (CEs) is of great importance for the increase of power conversion efficiency (PCE). Although Pt is the most widely used material for CEs of DSSCs, the high price and low abundance of Pt severely limit its application on a large scale and alternative materials are highly desired. In this paper, Bi$_2$Se$_3$ films of vertically aligned flake arrays fabricated by the vapor deposition technique are exploited as Pt-free CEs in DSSCs. Thanks to the excellent surface conductivity and the large number of catalytic active sites of Bi$_2$Se$_3$ flakes, the DSSC with a Bi$_2$Se$_3$ vertical flake array CE exhibited higher PCE than that with regular Pt CEs. This work provides an opportunity to develop practical Pt-free CEs which could facilitate the large-scale application of DSSCs.

Introduction

In the past two decades, dye-sensitized solar cells (DSSCs) have attracted considerable attention from the scientific community and the photovoltaic industry, owing to their low cost, simple production processes, environmental friendliness and high energy conversion efficiency.[1–3] As one of the elemental components in DSSCs, counter electrodes (CEs) are of great importance for the reduction rate of triiodide (I_3^-) to iodide (I^-).[4] Due to its chemical inertness, good conductivity and catalytic activity, Pt is conventionally used as the CE for catalyzing the reduction of I_3^-.[5] Nevertheless, Pt is a low-abundant element and consequently is extremely expensive, which prevents its large-scale application in DSSCs.[6,7] Therefore, great efforts have been devoted to finding proper substitutes for Pt in the past decade. So far, various materials like carbon nanotubes, conductive organic polymers and inorganic semiconductors have been proposed as Pt-free CEs.[4,8–12] However, none of them can completely replace Pt because of either low catalytic activity or poor chemical or thermal stability.

Recently, an exotic phase of matter, 3D topological insulators like Bi$_2$Se$_3$ and Bi$_2$Te$_3$, have been recognized as a promising material for various electrochemical applications, due to their novel laminar structure and topologically protected metallic surface states. For instance, Chen and his coworkers predicted

in their theoretical studies that Au covered topological insulators Bi$_2$Se$_3$ could show improved catalytic activity of CO oxidation because the surface states of Bi$_2$Se$_3$ would increase the adsorption energy of CO and O$_2$ molecules.[13] The electrochemical catalytic activity of the topological insulator Bi$_2$Se$_3$ were first demonstrated experimentally by applying the Bi$_2$Se$_3$ modified glass carbon electrode for the detection of glucose in human blood serum, in which the topological insulator facilitates the electron transfer at the interface.[14] Ali *et al.* have successfully synthesized the Bi$_2$Se$_3$ nanosheets by different synthesis methods and compared the electrochemical performance of various Bi$_2$Se$_3$ nanosheets as electrodes of lithium ion batteries for the first time.[15] Bi$_2$Se$_3$ can also be used as a potential electrochemical hydrogen storage material like other layered materials, such as MoS$_2$ and so on.[16,17] For example, excellent electrochemical hydrogen storage capacity and long cycle life under charge/discharge cycling of Bi$_2$Se$_3$ have been reported recently.[18] Although both theoretical and experimental studies indicate that Bi$_2$Se$_3$ has excellent electrochemical activity, to the best of our knowledge no research on the potential of using Bi$_2$Se$_3$ as CEs in DSSCs has been reported so far.

Herein, Bi$_2$Se$_3$ flake films were synthesized by vapor deposition on FTO substrate and were used directly as CEs in DSSCs. Electrochemical measurements show that the morphologies of the Bi$_2$Se$_3$ films will influence the catalytic activity of the CEs significantly. It is found that Bi$_2$Se$_3$ films composed of vertically aligned flake array exhibit outstanding electrocatalytic activity and could be a good candidate to replace Pt as CEs in DSSCs because of the unique surface conductivity and the abundant catalytic active sites of 3D topological insulators.

Centre for Advanced Optoelectronic Functional Materials Research, Key Laboratory for UV Light-Emitting Materials and Technology of Ministry of Education, Northeast Normal University, Changchun 130024, China. E-mail: majg@nenu.edu.cn; hyxu@ nenu.edu.cn; Fax: +86 85099772; Tel: +86 431 85099767

Experiments

Synthesis and preparation of CEs

The Bi_2Se_3 flakes were grown on FTO (OPV-FT022-7, America, transmittance 80–82%, square resistance 7–8 Ω, haze 5%, thickness 2.2 mm) by vapor deposition inside a horizontal vacuum tube furnace equipped with a 30 mm diameter quartz tube. The Bi_2Se_3 powder (5 N) was used as the source of the deposition. FTO substrates were placed at different temperature zones of the downstream away from the source. The tube is pumped down to a base pressure of 8×10^{-1} Pa and then flushed with Ar gas for several times. The Bi_2Se_3 powder was place at the center of the furnace and was heated up to 550 °C. Subsequently, the Ar was kept flowing at a rate of 65 sccm for 3 h. After the vapor deposition, the furnace was cooled down naturally. For comparison, Pt CEs were prepared by drop-casting 10 mol L^{-1} of chloroplatinic acid isopropyl alcohol solution on the surface of FTO substrates and subsequently annealing at 450 °C for 30 min.

Fabrication of DSSCs

A 10 μm thick layer of 20 nm sized TiO_2 particles (TiO_2 Paste DSL 18NR-T, Australia) was loaded on the FTO conducting glass by screen printer technique. After sintering at 125 °C, the obtained layer was further coated with a 6 μm thick scattering layer of 200 nm sized TiO_2 particles (OPV-TPP200, Yingkou) and sintered at 500 °C for 30 min. After that, the TiO_2 films on FTO glass were immersed in a solution of N719 (0.3 mM in aqueous ethanol) dye for 24 h to be used as the dye-sensitized photoanodes. The photoanodes and different CEs were assembled into a sandwich-type cell and separated by a 60 μm thick film (OPV-Surlyn-60, Yingkou) and sealed up. The cell interspace between the photoanode and CE was filled with the I^-/I_3^- redox electrolyte which is composed of 0.05 M LiI, 0.03 M iodine, 0.6 M 1,3-dimethylimidazolium iodide (DMII) ionic liquids, 0.1 M guanidinium thiocyanate (GuSCN), and 0.5 M 4-*tert*-butylpyridine in anhydrous acetonitrile: valeronitrile (85 : 15).[19,20] The assembled DSSCs were used to test the photocurrent–voltage (J–V) with an active area of 0.1256 cm^2. Identical DSSCs with an active area of 0.64 cm^2 were also assembled for electrochemical impedance spectroscopy (EIS) and Tafel-polarization (Tafel) measurements.

Characterization and measurements

The surface morphologies and the crystal structures of the Bi_2Se_3 CEs were characterized using a FEI Quanta 250 field-emission scanning electron microscope (SEM) and a Rigaku D/MAX 2500 PC X-ray diffractometer with Cu-Kα line radiation. XRD measurements were conducted in a conventional $\theta/2\theta$ scan mode. The current–voltage characteristics of the DSSCs were measured with a Keithley 2400 source meter under AM 1.5G simulated solar irradiation from a Sun 2000 solar simulator (ABET technology, 100 mW cm^{-2}). The EIS experiments and Tafel-polarization curves were measured in the dark using a Princeton PARSTAT 2273 advanced electrochemical system. 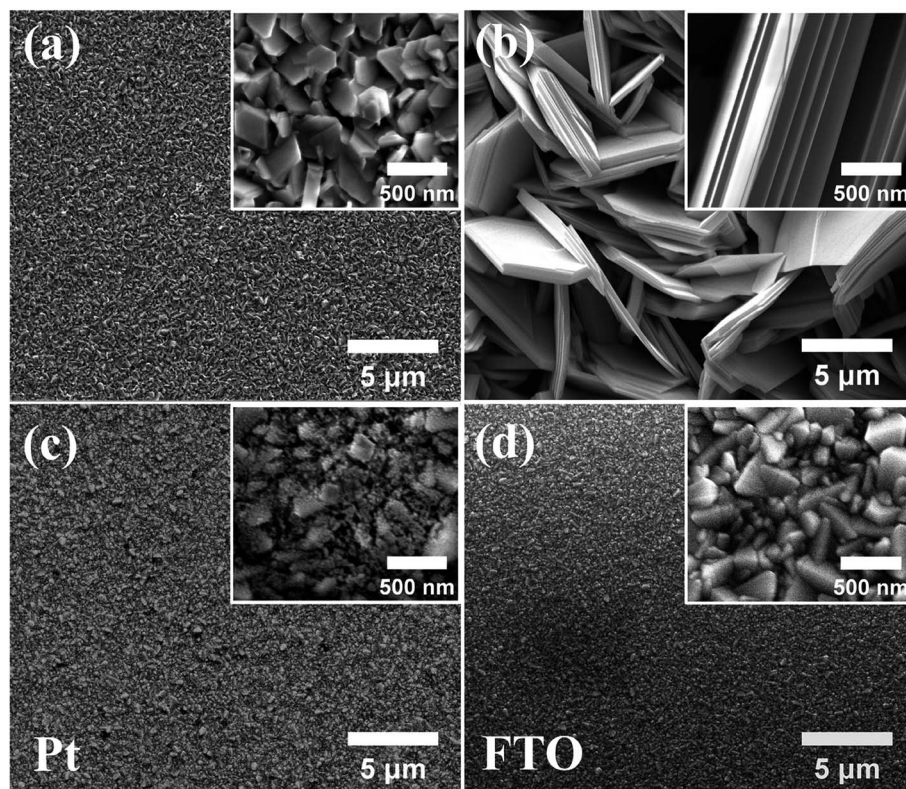EIS was recorded in the frequency range from 100 mHz to 100 kHz with an AC amplitude of 10 mV. The impedance measurements were carried out under a bias of 0 V in the dark. Tafel-polarization measurements were carried out under the bias between −1 to 1 V, with a scan rate of 50 mV s^{-1}.

Results and discussion

As reported previously, the surface morphology of Bi_2Se_3 nanostructures can be tuned by adjusting the substrate temperature and carrier gas flow rate through the vapor transport deposition.[21] Therefore, two substrates were placed at different temperature zones in order to obtain two typical Bi_2Se_3 nanostructures with different morphologies. Fig. 1(a and b) show the surface morphologies of the samples which were grown at 440 °C and 520 °C temperature zones, respectively. A pristine FTO substrate were shown in Fig. 1(d) for comparison purpose. It can be seen that when the substrate was placed at 440 °C temperature zone, a large number of submicron-sized Bi_2Se_3 flakes were obtained on the FTO substrate, while when the substrate was placed at 520 °C temperature zone, an array of upstanding micron-sized Bi_2Se_3 flakes were obtained. The surface morphology of the submicron-sized Bi_2Se_3 flake is in conformity with the FTO substrate, indicating that in the nucleation stage of their self-assembly Bi_2Se_3 flakes would rather grow along the facets of the FTO micro-crystals on the substrate. Since most of the area in Fig. 1(a) was covered by the terrace of the Bi_2Se_3 flakes, the sample in Fig. 1(a) is named as the terrace-terminated film. In contrast, the upstanding micron-sized Bi_2Se_3 flake array is composed of laminar Bi_2Se_3 flakes with numerous edges. So, the sample in Fig. 1(b) is named as the edge-terminated film. Fig. 1(c) shows the surface morphology of Pt coated FTO substrate, in which Pt nano-crystals can be observed in the valleys of FTO nano-crystals.

Fig. 2(a and b) show the XRD patterns of the terrace-terminated and the edge-terminated films, respectively. Except the peak from FTO substrate, all the peaks in the XRD patterns can be indexed as rhombohedral Bi_2Se_3 (JCPDS: 033-0214) which has a layered crystal structure composed of quintuple units stacking along the ⟨001⟩ direction. Since the XRD spectra were taken in the conventional $\theta/2\theta$ Bragg–Brentano geometry, only the crystal planes that are parallel to the substrate surface will produce diffraction peaks in the spectra, which would indicate the preferred orientation of nanostructures in the Bi_2Se_3 films with respect to the substrate surface. In Fig. 2(a) the strong diffraction peaks from (003) and (006) planes indicate that ⟨001⟩ direction is one of the preferred orientations for the terrace-terminated film. This is consistent with the crystal symmetry of Bi_2Se_3 and the surface morphology of the terrace-terminated film shown in Fig. 1(a), in which lots of flat Bi_2Se_3 terraces cover the surface of FTO substrate. In contrast, the edge-terminated film shows very weak (001) diffraction peak and strong (110) peak, indicating that the upstanding flakes in Fig. 1(b) tend to align along ⟨110⟩ direction which is perpendicular to the substrate surface. However, because the polycrystalline FTO substrates have a relative rough surface, the orientations of both the flat terraces and the upstanding flakes in Fig. 1(a and b) will somehow deviate from the normal of the
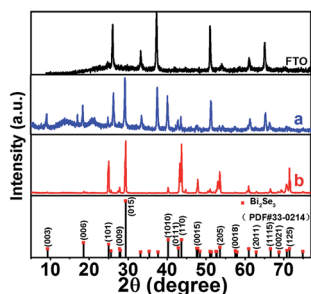
Fig. 1 The top-view SEM images of the Bi_2Se_3 films prepared by vapor deposition at 440 °C and 520 °C temperature zone, respectively (a and b). The top-view SEM image of Pt nano-crystals on the FTO substrate (c). The SEM image of a pristine FTO (d). The insets (a–d) are the corresponding magnified images.
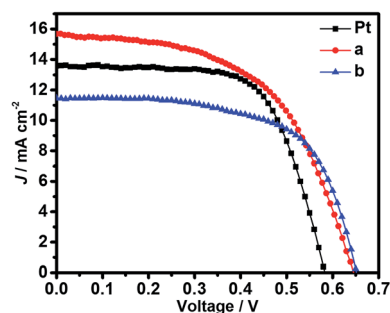
substrate, which is the main reason for the presence of other diffraction peaks such as (015) and (101) in the XRD spectra.

Fig. 3 shows the photocurrent density–voltage characteristics of N719-sensitized solar cells assembled with the conventional Pt (black square), the edge-terminated Bi_2Se_3 film (red circle) and the terrace-terminated Bi_2Se_3 film (blue triangle) as CEs, respectively. The relevant photovoltaic performance parameters including the short-circuit photocurrent density (J_{sc}), the open-circuit photovoltage (V_{oc}), the fill factor (FF) and the PCE derived from Fig. 3 are listed in Table 1. The DSSC with the edge-terminated Bi_2Se_3 film as CE the DSSC yielded a PCE of 5.52% ($J_{sc} = 15.67$ mA cm^{-2}, $V_{oc} = 0.65$ V, FF = 0.54), while the DSSC with the terrace-terminated Bi_2Se_3 film CE produced a PCE of 4.47% ($J_{sc} = 11.57$ mA cm^{-2}, $V_{oc} = 0.59$ V, FF = 0.65). For reference, a PCE of 5.25% ($J_{sc} = 13.60$ mA cm^{-2}, $V_{oc} = 0.58$ V, FF = 0.67) was obtained under the same condition for the DSSC with the conventional Pt CE. The standard deviation values of J_{sc}, V_{oc}, FF and PCE for the edge-terminated film were calculated to be 0.021, 0.585, 0.017 and 0.36, respectively. For the terrace-terminated Bi_2Se_3 CEs, the values are 0.005,

Fig. 2 (a and b) are $\theta/2\theta$ scan XRD patterns of the terrace-terminated film and the edge-terminated Bi_2Se_3 film grown at 440 °C and 520 °C, respectively. The diffractogram of FTO substrate and the standard PDF card of rhombohedral Bi_2Se_3 (PDF#00-033-0214) are shown as references.

Fig. 3 Photocurrent density–voltage characteristics of DSSCs with the conventional Pt, the edge-terminated films (curve a), and the terrace-terminated film (curve b) as CEs, measured at AM 1.5G illumination (100 mW cm^{-2}).

Table 1 Photovoltaic and electrochemical performance parameters for different CEs

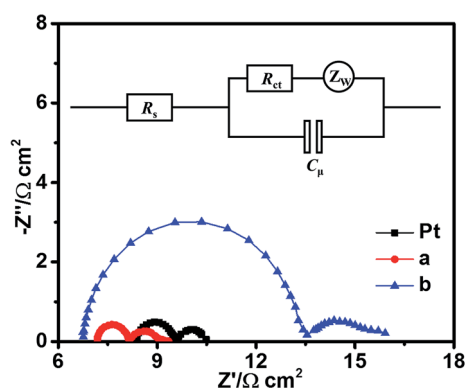| CE	V_{oc}/V	J_{sc}/mA cm^{-2}	FF	PCE/%	R_s/Ω cm^2	R_{ct}/Ω cm^2	C_μ/μF	CPE-P
Pt	0.58	13.60	0.67	5.25	8.40	1.11	17.9	0.94
Sample-a	0.65	15.67	0.54	5.52	7.20	0.92	20.9	0.99
Sample-b	0.65	11.46	0.63	4.71	6.75	6.64	9.2	0.95

0.158, 0.009 and 0.11 (Fig. S1 and Table S1†), respectively. The results show that both the edge-terminated film and the terrace-terminated film have good consistency of PCE performance. J_{sc} increased in the order of terrace-terminated film < Pt < edge-terminated film, and PCE increased in the same order. Obviously, the edge-terminated film performs even better than Pt as the CEs in DSSCs, indicating that upstanding Bi_2Se_3 flakes film possesses an excellent catalytic activity for the reduction of I_3^- ions to I^-.

To further evaluate the electrochemical characteristics of the Bi_2Se_3 CEs for the reduction of I_3^- ion, the EIS experiments were carried out using the symmetrical dummy cells with an active area of 0.64 cm^2. Fig. 4 shows the Nyquist plots for the symmetrical dummy cells with the conventional Pt, the edge-terminated and the terrace-terminated Bi_2Se_3 CEs. Two semicircles in the Nyquist plots can be observed in the high-frequency (left semicircle) and low-frequency (right semicircle) regions, respectively. Generally, the high-frequency intercept on the real axis (Z' axis) gives the series resistance (R_s) and the diameter of the semicircle in the high-frequency regions is assigned to the charge-transfer resistance (R_{ct}).[22] It is known that in EIS measurements the R_s value basically represent the ohmic resistance of the entire circuit including the resistance of CEs and FTO as well as other contact resistance, while the R_{ct} value is negatively proportional to the catalytic activity of the electrode on reduction of I_3^- ion.[23] C_μ is a constant phase element in the equivalent circuit diagram and typify the double-layer capacitance at the interface of CE/electrolyte due to the accumulation of ions on the electrode surface, which is
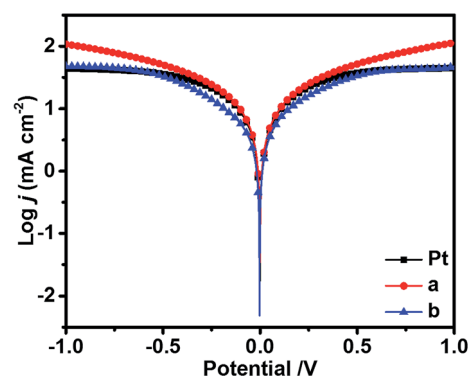
proportional to the active catalytic surface areas of CEs,[5,12] CPE-P is the degree of the dispersion. The EIS data including R_s, R_{ct} and C_μ were derived by fitting the Nyquist plots with Z-view software with the equivalent circuit diagram shown as the insert of Fig. 4.[4] The fitted results are also listed in Table 1.

Per the fit parameters of EIS data (see Table 1), the R_s values of cells with the edge-terminated and the terrace-terminated Bi_2Se_3 electrodes are 7.20 Ω cm^2 and 6.75 Ω cm^2, respectively, both of which are smaller than that of cell with Pt electrode (8.40 Ω cm^2), indicating that Bi_2Se_3 flake electrodes have better electrical conductivity than Pt electrode. However, it has been reported that the bulk resistivity of Bi_2Se_3 is two orders of magnitude higher than that of Pt (10.6 × 10^{-6} ohm cm).[24] According to Hall measurements, Bi_2Se_3 flake films have Hall mobilities of 510 cm^2 V^{-1} s^{-1} and 570 cm^2 V^{-1} s^{-1}, respectively, which are both higher than that of bulk material with the same carrier concentration.[25–27] Therefore, the small R_s value obtained with the edge-terminated and the terrace-terminated Bi_2Se_3 electrodes can be partially attributed to the transportation by a topologically protected surface state rather than the transportation in the bulk of Bi_2Se_3 alone.[14] As shown in Table 1, the R_{ct} values with the Pt, the edge-terminated and the terrace-terminated Bi_2Se_3 electrodes are 1.11, 0.92, and 6.64 Ω cm^2, respectively. The edge-terminated Bi_2Se_3 CE gives the minimum R_{ct} value among all the CEs, indicating that the edge-terminated Bi_2Se_3 films have the best catalytic activity among the three electrodes.

To further investigate the electrochemical characteristics of Bi_2Se_3 and Pt electrodes, the Tafel polarization curves were measured on the symmetrical cells used in EIS experiments, as shown in Fig. 5. It shows the current density (J) as a function of voltage (V) at room temperature for the reduction of I_3^- to I^-.

Fig. 4 Nyquist plots for the symmetric cells with the edge-terminated (red circles) and the terrace-terminated Bi_2Se_3 films (blue triangles) as CEs. Pt CE was also presented for reference (black squares). The EIS were measured with a frequency range from 100 kHz to 100 mHz, and the amplitude of the alternating current was set to 10 mV. Insert is the equivalent circuit diagram.

Fig. 5 Tafel polarization curves of the I_3^-/I^- symmetrical cells fabricated with the edge-terminated films (red curve), the terrace-terminated films (blue curve) and the Pt (black curve) different CEs.

The slopes of the tangent to the anodic or cathodic branches are in the order of edge-terminated film > Pt > terrace-terminated film. A large slope in the anodic or cathodic branches indicates a higher exchange current density (J_0) on the electrode. Therefore, the edge-terminated film has the best catalytic activity.

On the other hand, J_0 can also be calculated by the following eqn (1).

$$J_0 = \frac{RT}{nFR_{ct}} \qquad (1)$$

where R is the gas constant, T is the absolute temperature, F is the Faraday's constant, R_{ct} is obtained from EIS spectra (Fig. 4) and n is the number of electrons involved in the electrochemical reduction of I_3^- at the electrode, which is 2 in our case. Because the R_{ct} values of cells with various electrodes increase in the order of the edge-terminated films < Pt < the terrace-terminated films, J_0 calculated by eqn. 1 decrease correspondingly in reverse order, which is consistent with the results extracted from the Fig. 5.

Because the surface morphologies of the edge-terminated, the terrace-terminated Bi_2Se_3 films and the Pt CEs are so different from each other, it is necessary to evaluated the active catalytic surface areas of each CE by comparing the equivalent capacitance C_μ. The relevant degree of the dispersion (CPE-P) are all above 0.9. Therefore, C_μ can be regarded as a pure capacitor. As show in Table 1, the C_μ of the edge-terminated Bi_2Se_3 film (20.9 μF) is 10% larger than that of the Pt (17.9 μF) and is one time larger than that of the terrace-terminated Bi_2Se_3 electrodes (9.2 μF). The edge-terminated Bi_2Se_3 film CE has the largest active catalytic surface area, which could be tentatively ascribed to the special structure of upstanding micron-sized flake array.

As can be seen in Fig. 1, the edge-terminated Bi_2Se_3 film is composed of upstanding flakes with lengths of sides up to several microns, while the terrace-terminated film is composed of lying flakes whose sizes are about ten times smaller than that of the edge-terminated Bi_2Se_3 film. On the other hand, the cross-sectional SEM image (no shown here) indicated that the height of the upstanding flake of the edge-terminated film is in the range of 5–8 microns and both sides of each flake are exposed and consequently could contact with the electrolyte. Then, the ratio of total contact surface area to the substrate area of 41 and 1.4 for the edge-terminated (Fig. 1(b)) and the terrace-terminated samples (Fig. 1(a)), respectively. In spite of the distinct difference of the ratios between the two series of samples, the C_μ of the edge-terminated Bi_2Se_3 CE is only two times of that of the terrace-terminated Bi_2Se_3 CE. Therefore, we think that not all the contact surface will contribute equally to the catalytic activity of Bi_2Se_3 CEs, but the amount of active sites like steps and edges will make a difference.

It is shown in XRD spectra that both the edge-terminated and the terrace-terminated Bi_2Se_3 films have rhombohedral structure which has a six-fold symmetry along the ⟨001⟩ direction. So, the hexagonal terraces of the flakes in Fig. 1 should belong to the {001} planes and the six lateral rectangle facets should belong to the {100} planes of Bi_2Se_3.[21] It is known that
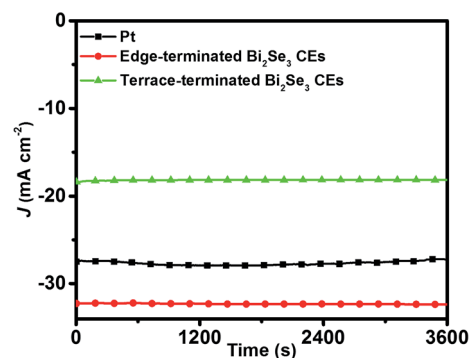

Fig. 6 Current density *vs.* time plots of Pt and Bi_2Se_3 CEs under −0.25 V bias voltage.

{001} planes have the lowest surface energy among all the crystal planes of Bi_2Se_3 and catalytic reactions will most likely take place at planes with high surface energy.[28] Although both the surface area of {001} and {100} planes increased with the increasing size and thickness of flakes in the edge-terminated film, the catalytic activity will mainly benefit from the increase of {100} surface area.

Furthermore, it can be noticed in the inset of Fig. 1(b) that there are many steps that can be observed at edges of upstanding Bi_2Se_3 flakes, which is common for vapor deposition of materials with laminated structures. Since the Bi_2Se_3 flakes were constructed by stacking Bi_2Se_3 quintuple layers, the fluctuation of growth rate in different layers results in the presence of steps near the edge of the flakes. With the increasing size and thickness of flakes the number of steps
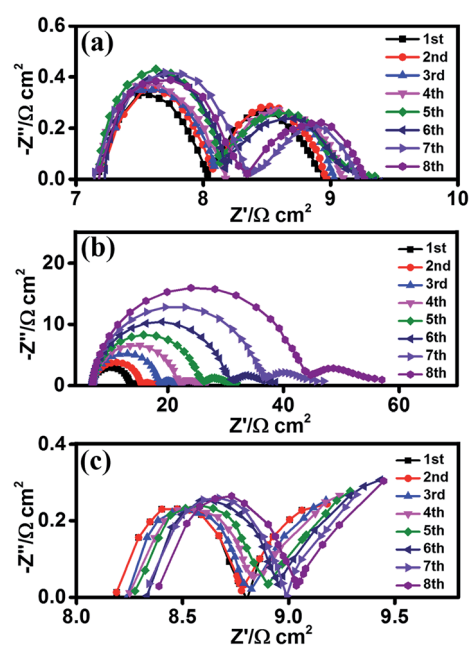

Fig. 7 Nyquist plots of EIS for the symmetrical cells with the edge-terminated Bi_2Se_3 sample-a (a), the terrace-terminated Bi_2Se_3 sample-b (b), and Pt (c) CEs. EIS tests at 0 V from 100 kHz to 100 mHz was performed continuously for 8 times.

will increase consequently. Considering that the steps could have even higher free energies than the adjacent planes, one can expect that I_3^- ions could be efficiently reduced to I^- at the active sites of those steps. Therefore, the high catalytic activity of the edge-terminated Bi_2Se_3 film can be attributed to the increase of both the surface area of {100} planes and the length of steps.

Since stability is one of the most important factors for the practical application of CE,[4,29,30] we performed successive current–time and EIS tests to examine the stability of the edge-terminated film and the terrace-terminated film of Bi_2Se_3 flakes CEs. During the current–time test, the current density of the edge-terminated film and terrace-terminated film of Bi_2Se_3 flakes CEs maintained 99.7 and 98.7% of the original current after 3600 seconds at −0.25 V, respectively (Fig. 6). The EIS tests on dummy cells were conducted for 8 cycles, after which there was negligible change in R_{ct} for the edge-terminated Bi_2Se_3 and Pt CEs. However, R_{ct} increased from 6.64 to 23.44 Ω cm^2 for the terrace-terminated Bi_2Se_3 CEs (Fig. 7(b)), due to Bi_2Se_3 flakes peeling off from the FTO surface during the tests. In addition, R_s is almost unchanged for all the samples, meaning that the continuous cycling hardly influenced the series ohm resistance.

Conclusions

In summary, the edge-terminated film and terrace-terminated film of Bi_2Se_3 flakes have been grown on the surface of FTO through vapor transport deposition and are exploited as CEs in DSSCs. SEM, XRD, PCE and EIS measurements indicate that the edge-terminated film of Bi_2Se_3 flakes exhibit a better catalytic activity for the reduction of I_3^- than the Pt CE. It is found that the superior catalytic activity of the edge-terminated Bi_2Se_3 CE can be understood from two aspects. One is the increase of active sites with the increasing surface area of {100} planes and the length of steps that have higher surface energy. The other is the good charge transportation though the topologically protected surface states of Bi_2Se_3 flakes. The unique structure of upstanding Bi_2Se_3 flake array is a good example for utilizing layered topological insulator as effective catalytic materials.

Conflicts of interest

There are no conflicts to declare.

Acknowledgements

References

1 B. O'Regan and M. Grätzel, Nature, 1991, 353, 737–740.

2 M. Grätzel, Nature, 2001, 414, 338–344.

3 A. Hagfeldt, G. Boschloo, L. Sun, L. Kloo and H. Pettersson, Chem. Rev., 2010, 110, 6595–6663.

4 F. Gong, H. Wang, X. Xu, G. Zhou and Z.-S. Wang, J. Am. Chem. Soc., 2012, 134(26), 10953–10958.

5 Y. Hou, D. Wang, X. H. Yang, W. Q. Fang, B. Zhang, H. F. Wang, G. Z. Lu, P. Hu, H. J. Zhao and H. G. Yang, Nat. Commun., 2013, 4, 1583.

6 N. Papageorgiou, Coord. Chem. Rev., 2004, 248, 1421–1446.

7 G. Calogero, P. Calandra, A. Irrera, A. Sinopoli, I. Citro and G. Dimarco, Energy Environ. Sci., 2011, 4, 1838–1844.

8 A. Kay and M. Grätzel, Sol. Energy Mater. Sol. Cells, 1996, 44, 99–117.

9 F. Gong, H. Wang and Z.-S. Wang, Phys. Chem. Chem. Phys., 2011, 13, 17676–17682.

10 Q. H. Li, J. H. Wu, Q. W. Tang, L. Zhang, P. J. Li, J. M. Lin and L. Q. Fan, Electrochem. Commun., 2008, 10, 1299–1302.

11 G. R. Li, J. Song, G. L. Pan and X. P. Gao, Energy Environ. Sci., 2011, 4, 1680–1683.

12 M. Wu, X. Lin, A. Hagfeldt and T. Ma, Angew. Chem., Int. Ed., 2011, 50, 3520–3524.

13 H. Chen, W. Zhu, D. Xiao and Z. Zhang, Phys. Rev. Lett., 2011, 107(5), 056804.

14 S. Chen, Y. M. Fang, J. Li, J. J. Sun, G. N. Chen and H. H. Yang, Biosens. Bioelectron., 2013, 46, 171–174.

15 Z. Ali, C. Cao, J. Li, Y. Wang, T. Cao, M. Tanveer, M. Tahir, F. Idrees and F. K. Butt, J. Power Sources, 2013, 229, 216–222.

16 J. Chen, N. Kuriyama, H. Yuan, H. T. Takeshita and T. Sakai, J. Am. Chem. Soc., 2001, 123, 11813–11814.

17 B. Zhang, X. C. Ye, W. Dai, W. Y. Hou and X. Yi, Chem.–Eur. J., 2006, 12, 2337–2342.

18 Z. Sun, S. Liufu, X. Chen and L. Chen, Chem. Commun., 2010, 46, 3101–3103.

19 P. Sun, X. Zhang, L. Wang, F. Li, Y. Wei, C. Wang and Y. Liu, New J. Chem., 2015, 39(6), 4845–4851.

20 Z. Jin, Y. Wang, S. Chen, G. Li, L. Wang, H. Zhu, X. Zhang and Y. Liu, RSC Adv., 2016, 6(13), 10450–10455.

21 M. Han, J. Ma, H. Xu and Y. Liu, CrystEngComm, 2015, 17(44), 8449–8456.

22 F. Fabregat-Santiago, J. Bisquert, E. Palomares, L. Otero, D. Kuang, S. M. Zakeeruddin and M. Grätzel, J. Phys. Chem. C, 2007, 111, 6550–6560.

23 J. Chen, K. Li, Y. Luo, X. Guo, D. Li, M. Deng, S. Huang and Q. Meng, Carbon Balance Manage., 2009, 47, 2704–2708.

24 J. Suh, D. Fu, X. Liu, J. K. Furdyna, K. M. Yu, W. Walukiewicz and J. Wu, Phys. Rev. B: Condens. Matter Mater. Phys., 2014, 89, 115307.

25 P. Janíček, Č. Drašar, L. Beneš and P. Lošťák, Cryst. Res. Technol., 2009, 5, 505–510.

26 K. Jacob John, B. Pradeep and M. Elizabeth, *Solid State Commun.*, 1993, **85**(10), 879–881.

27 F.-T. Huang, M.-W. Chu, H. H. Kung, W. L. Lee, R. Sankar, S.-C. Liou, K. K. Wu, Y. K. Kuo and F. C. Chou, *Phys. Rev. B: Condens. Matter Mater. Phys.*, 2012, **86**, 081104.

28 S. Wang, H. Chen, G. Gao, T. Butburee, M. Lyu, S. Thaweesak, J. Yun, A. Du, G. Liu and L. Wang, *Nano Energy*, 2016, **24**, 94–102.

29 L. Kavan, J. H. Yum and M. Grätzel, *ACS Nano*, 2011, **5**, 165–172.

30 S. Lu, Y. Wang, F. Li, G. Yang, H. Yang, X. Zhang and Y. Liu, *J. Phys. Chem. C*, 2017, **121**, 12524–12530.